Highly-Scalable Transmission and Distribution Dynamic Co-Simulation with 10,000+ Grid-Following and Grid-Forming Inverters

Yuan Liu, *Member, IEEE*, Renke Huang, *Senior Member, IEEE*, Wei Du, *Senior Member, IEEE*, Ankit Singhal, *Member, IEEE*, Zhenyu Huang, *Fellow, IEEE*

***Abstract*—The inverter-based resource (IBR) has been an important component of power generation within both transmission and distribution systems. The impacts of high IBR penetration on system transient stability have not been explored extensively due to the lack of high-fidelity power grid and inverter models. The aggregate IBR model in the transmission system is only suitable for representing bulk power system (BPS)-connected IBRs, and it cannot precisely reproduce the dynamics of distributed IBRs in the distribution system due to its oversimplified structure. In this study, we have developed a high-penetration fully-connected transmission and distribution (T&D) co-simulation platform that supports the dynamic co-simulation of a synthetic mini-WECC transmission system with multiple IEEE 8500-node distribution systems. The entire platform can accommodate 10,000+ dispersed and 40+ BPS-connected IBRs and achieve 100% power generation from IBRs. A novel iterative T&D power flow initialization technique was proposed to maintain stable transition from power flow to dynamic co-simulation mode with high penetration of IBR models. This study explores the impacts of grid-forming (GFM) and grid-following (GFL) inverter control on the dynamics of large-scale T&D network. Moreover, a co-simulation platform was developed and tested using high-performance computing (HPC) resources to facilitate parallel simulation.**

***Index Terms*—Co-simulation, Grid-forming control, High-performance computing, Inverter-based resources, Phasor-domain**

I. Introduction

The advent of power electronics technology has been reshaping the various aspects of current electric power infrastructure ranging from power generation, transmission to distribution, and even end-use consumption. The wind and solar power plants, battery energy storage systems (BESSs) and variable frequency drive (VFD) loads rely on power electronic inverters as the interface to the higher-level *ac* power grid. As the contribution of inverter-based renewable energy toward electricity generation gradually increases, the development of a grid-friendly control design becomes essential for the reliable operation and production of power by inverter-based resources (IBRs).

Most of the current IBRs are configured with grid-following (GFL) control that relies on phase-locked loop (PLL) unit to synchronize with grid frequency and control the inverter terminal current components [1]. However, the IBRs with GFL control and PLL are bound to encounter instability issues as the penetration increases or when they are operated in weaker power grids. Under these circumstances, the concept of grid-forming (GFM) control has been proposed and it has been drawing extensive attention from the industry. Unlike GFL inverters that regulate their own currents regardless of grid conditions, the inverters with GFM technology will be directly controlled to adjust the frequency and magnitude of the output *ac* voltage and behave as a controllable voltage source behind impedance to enhance the stability of the power grid. The distribution system dynamics with GFM-controlled inverters have been thoroughly studied and described in a recent study [1]. Several recent studies discussed the model aggregation using dynamic equivalencing methods for distribution systems that contained IBR generation [2]–[5]. Authors in [3] reviewed historical and current methods for creating dynamic equivalent in electro-magnetic transient (EMT) domain. Rabuzin and group [4] considered phasor-domain modeling, and model structure and selection with different classes of system events when generating dynamic equivalent models. Authors in [5] focused on artificial intelligence (AI) -based dynamic equivalencing approaches. Authors in [6] proposed a modified gray-box equivalent model identification technique for representing the dynamics of a given active distribution network and considered its interoperability with transmission system. Though model simplification by dynamic equivalencing methods reduces model complexity and improves simulation efficiency, the impacts of distributed GFM- and GFL- controlled IBRs on transmission system dynamics have not been fully investigated using aggregate models generated by dynamic equivalencing. This paper fills this knowledge gap by focusing its efforts on developing a large-scale transmission and distribution (T&D) network with high-penetration of distributed IBRs.

Full EMT model for the entire transmission network has been developed in some industry practices to better simulate the system behaviors with the advent of high IBR penetration. For example, the Australian Energy Market Operator

Pacific Northwest National Laboratory (PNNL) is operated by Battelle for the U.S. Department of Energy (DOE) under Contract DE-AC05-76RL01830. This work was funded through PNNL's Laboratory Directed Research and Development (LDRD) program and DOE's Universal Interoperability for Grid-Forming Inverters (UNIFI) Consortium. This material is based upon work supported by the U.S. Department of Energy's Office of Energy Efficiency and Renewable Energy (EERE) under Solar Energy Technologies Office (SETO) Award Number 38637. The views expressed herein do not necessarily represent the views of the U.S. Department of Energy or the United States Government. (*Corresponding author: Wei Du*)

Y. Liu, W. Du, and Z. Huang are with PNNL, Richland, WA 99354, USA (e-mail: {yuan.liu, wei.du, zhenyu.huang}@pnnl.gov). R. Huang is with Shanghai Jiao Tong University, China (e-mail: huangrenke@gmail.com). A. Singhal is with Indian Institute of Technology (IIT), Delhi, India (e-mail: sankit@ee.iitd.ac.in).

(AEMO) has developed wide-area models of the National Electricity Market (NEM) power system by leveraging EMT and real-time digital simulators such as PSCAD and OPAL-RT [7]. However, this development effort still cannot cover the distribution networks. Recently, the U.S. Department of Energy (DOE) funded two thrusts to develop co-simulation engines, including Framework for Network Co-simulation (FNCS) and Hierarchical Engine for Large-scale Infrastructure Co-Simulation (HELICS) [8], [9]. The advanced co-simulation engines stimulate the research and development of interconnecting cross-domain simulation tools [10]. The T&D co-simulation studies have been implemented across different domains. Huang and group have summarized and compared the interface techniques for T&D dynamic co-simulation and suggested proper interface models (e.g., voltage or current source, Thevenin or Norton equivalent), taking into consideration if the transmission network is a positive-sequence or three-sequence transient stability model and whether distribution system uses power flow (PF) or dynamic simulation model [11].

Numerous studies have attempted to investigate power flow co-simulation integrating transmission and distribution systems. Balasubramaniam and colleague have proposed a quasi-static time series (QSTS) power flow co-simulation framework to assess the impacts of distribution-side Volt/VAR control on transmission system [12]. Yip and co-authors have developed joint T&D power flow methods to study the dependence of transmission voltage on the location of photovoltaic (PV) and electric vehicle (EV) [13]. Bharati and colleague have proposed an iterative power flow co-simulation algorithm to investigate system voltage stability margin with distributed generation (DG) penetration [14]. Jain and group [15] have leveraged an integrated grid modeling system (IGMS) [16] to co-simulate the T&D power flow. Panossian and colleagues have also developed a tightly-coupled T&D power flow co-simulation platform interfacing PowerWorld and OpenDSS through HELICS [17]. Sadnan and group have proposed decoupled, loosely-coupled and tightly-coupled T&D QSTS power flow co-simulation algorithms and compared the performances of these three coupling methods [18], while Krishnamoorthy from the same group of researchers has proposed an iterative coupling method for this T&D co-simulation platform [19].

Other researchers have co-simulated positive sequence (Pos.-Seq.) transmission network with three-phase phasor-domain distribution network. Venkatraman and group have integrated PSAT and OpenDSS to compare the performances of composite load model (CLM) and detailed distribution feeder model and have provided guidance for CLM parameter tuning [20]. The distribution side is represented by iterative power flow solution considering the differential algebraic equations (DAEs) of nodal-level dynamic components [21]. Kenyon et al. have developed a coupled T&D co-simulation to study DG response to transmission-side power system faults [22]. In that study, dynamic simulation was used for the transmission-side PSLF model while the QSTS power flow simulation was performed for the distribution-side OpenDSS model. An iterative method was used to combine both simulations and guarantee convergence and accuracy of the co-simulation model. In a recent publication, Rezvani and group have proposed a coupled load flow algorithm and dynamic simulation algorithm to enable T&D co-simulation [23]. However, the distribution side reported still had a power flow representation rather than true dynamic simulation. Bharati et al. have implemented a PSS/E – GridLAB-D dynamic co-simulation platform to study the impacts of distribution-side induction motor loads on transmission system dynamics [24]. However, most commercial transient stability simulation tools may not be appropriate to perform very large-scale T&D co-simulations because of: a) the lack of co-simulation engine and interface models in these tools, b) incompatibility with high-performance computing (HPC) operating systems and parallel computing platforms, and c) inaccessibility to the source code if the implementation of iterative algorithms is required for improving accuracy. Wang and co-authors developed a co-simulation platform to study the frequency and voltage responses of distributed energy resource (DER) penetration using transmission simulator ANDES, distribution simulator OpenDSS, and co-simulation engine HELICS [25]. However, the distribution system in Wang's work was simulated using QSTS power flow model at 1s communication interval with the transmission system. Therefore, the electro-mechanical dynamics (in the timescale of milli-seconds) and distributed inverter dynamic models were not present in the distribution systems in Wang's paper. The co-simulation platform developed in [26] leveraged FNCS to interface GridPACK and GridLAB-D [27], [28], which represents the dynamic co-simulation between positive sequence transmission network and 3-phase phasor-domain distribution networks. The scalability of the test system described in the above-mentioned work was relatively small and the inverter model used was a simple PV inverter.

Several studies have investigated the co-simulation between phasor-domain transmission network and electro-magnetic transient (EMT) distribution networks [29], [30]. A novel three-sequence/three-phase (3-Seq./3-Ph.) co-simulation platform was proposed to directly interface phasor-domain three-sequence transmission network with three-phase distribution networks [31]. Wang and group have presented a T&D co-simulation platform linking the phasor-domain transmission simulator power system analysis software package (PSASP) and EMT-domain distribution simulator PowerFactory using TCP/IP communication protocol [32]. Authors in [33] and [30] have extended the transmission system from positive sequence to three sequence and co-simulated it with EMT distribution system to handle unbalanced fault.

TABLE I summarizes the T&D side simulation tools, power grid models, simulation algorithms, and co-simulation coordination interfaces reported in the reviewed papers.

Our study significantly extends the scope of the work in [26] by using the next-generation co-simulation engine HELICS, parallel computation platform, large-scale transmission and distribution networks in GridPACK and GridLAB-D, and advanced inverter models with GFL and GFM control on both T&D sides. The 120-bus mini-WECC system [34] was used as the transmission network and the IEEE 8500-node test feeder was used as the distribution network. The co-simulation plat-

TABLE I
SUMMARY OF LITERATURE REVIEW

Ref.	Trans. Simulator	Trans. Model	Dist. Simulator	Dist. Model	Trans. Algo.	Dist. Algo.	Co-sim. Interface
[12]	MatPower	IEEE 118-bus	GridLAB-D	2 IEEE 13-node feeders	QSTS/PF	QSTS/PF	TCP socket
[13]	PSS/E	IEEE 30-bus	OpenDSS	12 IEEE 34-node feeders at one bus	QSTS/PF	QSTS/PF	Python wrapper
[14]	PyPower	IEEE 118-bus	GridLAB-D	IEEE 123-node feeders at 5 buses	QSTS/PF	QSTS/PF	Python wrapper
[15]	MatPower & FESTIV	PJM 5-bus	GridLAB-D	5 Taxonomy feeders	QSTS/PF	QSTS/PF	ZeroMQ
[17]	PowerWorld	Austin 173-bus	OpenDSS	feeders at 120 buses	QSTS/PF	QSTS/PF	HELICS
[18]	MATLAB	IEEE 39-bus	OpenDSS	EPRI Ckt-24 feeders at 10 buses	QSTS/PF	QSTS/PF	MATLAB
[20]	PSAT	IEEE 9-bus	OpenDSS	160-node feeder at one bus	Pos.-Seq. Dynamic	QSTS/PF	MATLAB
[22]	PSLF	WECC	OpenDSS	123 California feeders	Pos.-Seq.	QSTS/PF	N/A
[23]	MATLAB	Equivalent system (<10 buses)	OpenDSS	3-node feeder	Pos.-Seq. Dynamic	QSTS/PF	MATLAB
[24]	PSS/E	IEEE 118-bus	GridLAB-D	IEEE 123-node feeders at 5 buses	Pos.-Seq. Dynamic	3-Ph. Dynamic	HELICS
[32]	PSASP	Real system (>30,000 buses)	PowerFactory	1 real feeder (<200 nodes) at one buse	Dynamic	EMT	TCP/IP protocol
[33],[30]	InterPSS	WECC	PSCAD	An area with 238 buses	3-Seq. Dynamic	EMT	PSCAD TCP/IP socket
[25]	ANDES	ACTIVSg2000 (Texas 2000-bus)	OpenDSS	243 feeders	Pos.-Seq. Dynamic	QSTS/PF	HELICS
[26]	GridPACK	IEEE 39-bus	GridLAB-D	IEEE 13-node feeders at 7 buses	Pos.-Seq. Dynamic	3-Ph. Dynamic	MATLAB

form we developed can handle 10,000+ small-scale distributed inverter models and 40+ BPS-connected aggregate renewable generator models. Unstable initialization could result in numerical divergence during dynamic simulation given high IBR penetration. To maintain numerical stability of such a huge co-simulation network, an iterative T&D power flow initialization has been proposed to seamlessly interface GridPACK and GridLAB-D at the initiation of the co-simulation and flat-start the dynamic co-simulation. The contributions of this paper are highlighted below.

- A new iterative T&D power flow initialization method was invented to update the boundary conditions of interface buses on both T&D sides to eliminate the start-up dynamics of the co-simulation.
- According to the literature review as of now, this work develops the largest phasor-domain T&D co-simulation model (measured by number of distribution feeders and nodes) with electro-mechanical dynamics on both T and D sides.
- Advanced GFM inverter models with droop control and overload control were developed in both the positive-sequence and three-phase phasor simulation tools. The freq-watt and volt-var controls of distribution-side GFL inverters were implemented.
- Compared with other literature, the largest number of small-scale inverters were modeled in the dynamic co-simulation at milli-seconds simulation and communication interval between transmission and distribution systems.
- As an extreme case of high IBR penetration, the case of 100% IBR generation was designed and successfully implemented as a part of this study to investigate the minimum percentages of GFM inverters required to maintain power system dynamic stability. The authors would like to emphasize that the 100% IBR generation case is not realistic for the WECC system because it contains a lot of hydro-power plants. However, the 100% IBR generation case might happen in some other systems. Therefore, it would be beneficial to explore the 100% IBR case from the research perspective using the developed T&D co-simulation platform, although it is not realistic for the WECC system. The developed T&D co-simulation platform and inverter models can be used to study any power system systems, and the authors selected the WECC system as a specific use case.

II. INVERTER MODEL DEVELOPMENT

This section presents the details of inverter model development including transmission-side and distribution-side inverter models, and grid support functions of distribution-side GFL inverters.

A. Transmission-Side Inverter Models

Both GFM and GFL inverter models were developed in the transmission simulator GridPACK. The Western Electricity

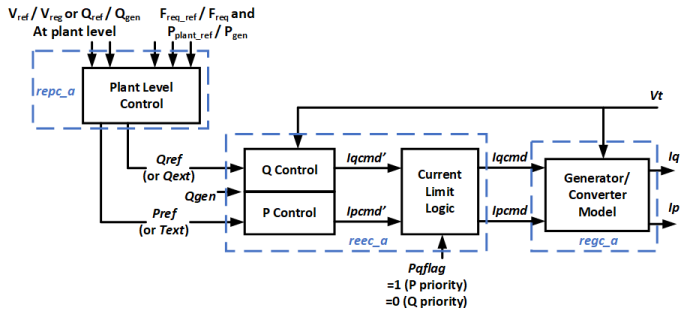

Fig. 1. Grid-following control (generic renewable model) - positive sequence simulator.

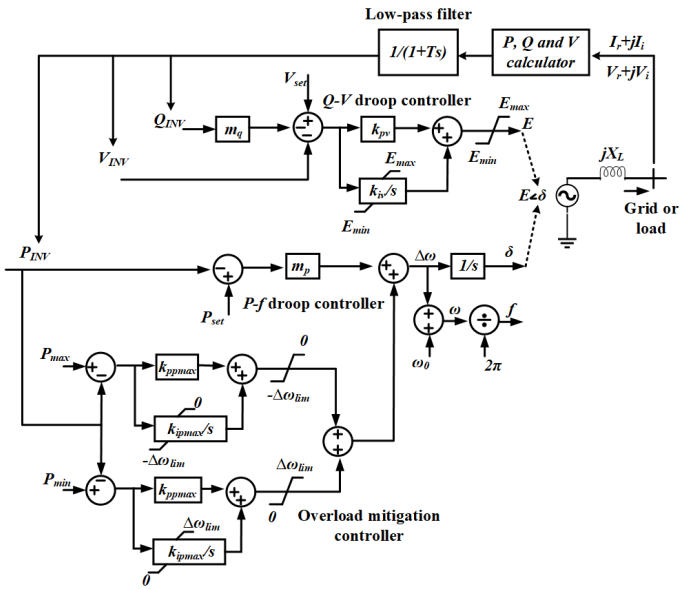

Fig. 2. Grid-forming control - positive-sequence phasor-domain simulator.

Coordinating Council (WECC) generic renewable model is a representative GFL inverter model, comprising of a combination of three modules shown in Fig. 1 [35]. This figure shows the dynamic representation of a bulk power system (BPS) - connected aggregate IBR. As shown in the figure, the plant control module REPC_A monitors the point of interconnection (POI) and gives real and reactive power command to the electrical control module REEC_A at individual generation unit level to control their real and reactive power output. Thereafter, the REEC_A module then processes this input, feedback of terminal voltage, and generator power output and then issues real and reactive current command to the generator/converter REGC_A module. Based on this command, REGC_A module injects current into the grid. Out of these three control modules, only the generator/converter model can run a simulation, other modules are needed for control functionality.

The transmission-side GFM inverter is a positive sequence model including Q–V droop control, P–f droop control and overload mitigation control, as shown in Fig. 2 [36]. The inverter terminal power and voltage magnitude can be calculated from the voltage and current phasors by Eq. (1) - Eq. (3). The control inputs P_{INV}, Q_{INV} and V_{INV} are measured signals by passing the calculated P, Q, V values through a low-pass filter representing measurement delay.

$$P_{INV} = \frac{1}{1+Ts}(V_r I_r + V_i I_i) \tag{1}$$

$$Q_{INV} = \frac{1}{1+Ts}(V_i I_r - V_r I_i) \tag{2}$$

$$V_{INV} = \frac{1}{1+Ts}\sqrt{V_r^2 + V_i^2} \tag{3}$$

In Q–V droop control, V_{INV} is tracked to a reference voltage obtained from droop, $V_{set} - m_q * Q_{INV}$, via a proportional integral (PI) controller (proportional and integral gains as k_{pv} and k_{iv}) by generating an appropriate internal voltage magnitude, E. Similarly, in P–f droop control, angular frequency reference, ω, is generated based on the deviation of inverter power, P_{INV} from the set-point of droop curve, P_{set}. The overload mitigation control provides a correction signal to frequency in case P_{INV} exceeds the minimum (P_{min}) and maximum (P_{min}) possible power of inverter such that P_{INV} remains at the P_{min} or P_{max}. When P_{INV} is within the limit, the correction becomes 0 as shown in Fig. 2. It is noted that k_{ppmax} and k_{ipmax} are the proportional and integral gain of P_{max} and P_{min} controller.

B. Distribution-Side Inverter Models

The distribution-side three-phase GFM inverter, as shown in Fig. 3, basically uses the same controllers as the positive-sequence inverter model in Fig. 2 and generates three-phase voltage signals at the outputs. The active power (P_{INV}) and reactive power (Q_{INV}) inputs of the controllers are obtained by passing the total power of all phases (P_k, Q_k) via a low pass filter (time constant T) as shown in Eq. (4) and (5) where $k \in \{a, b, c\}$ denotes the phase. The voltage magnitude input (V_{INV}) takes the average of three-phase voltage magnitudes passed through the low-pass filter, calculated using the Eq. (6). The phase angles of the internal three-phase voltages, δ_k, can be obtained using Eq. (7), where δ is the output of the P–f droop control. It should be noted that the internal voltages are three-phase balanced.

$$P_{INV} = \frac{1}{1+Ts}(P_a + P_b + P_c)/S_B \tag{4}$$

$$Q_{INV} = \frac{1}{1+Ts}(Q_a + Q_b + Q_c)/S_B \tag{5}$$

$$V_{INV} = \frac{1}{3(1+Ts)}(V_{ga} + V_{gb} + V_{gc})/V_B \tag{6}$$

$$[\delta_a, \delta_b, \delta_c] = [\delta, \delta, \delta] + [0, -2\pi/3, 2\pi/3] \tag{7}$$

$$E_a = E_b = E_c = E \tag{8}$$

The GFL inverter model developed in distribution-side simulator GridLAB-D can be single- or three-phase. In this study, we assume the GFL inverter is three-phase and outputs balanced currents to the grid. The GFL controllers include two key components, the PLL and the current control loop. The most important aspect of GFL control is to synchronize the inverter output to the grid voltage reference frame. To

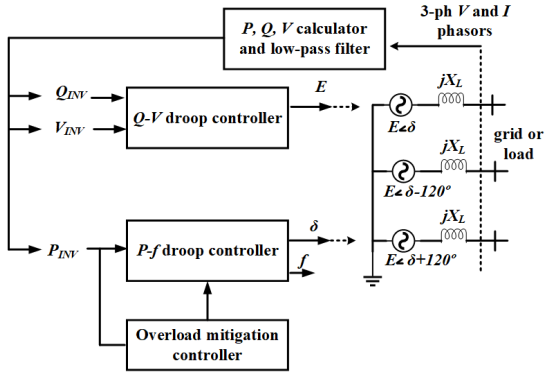

Fig. 3. Grid-forming control in three-phase phasor-domain simulator.

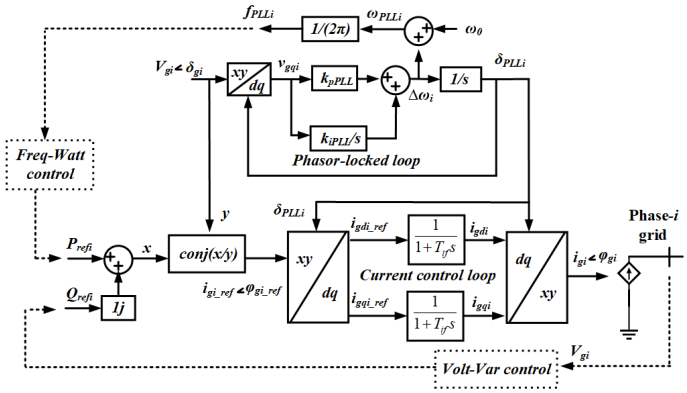

Fig. 4. Grid-following control in three-phase phasor-domain simulator - one of the three phases (*Note: the other two phases are identical in structure*).

achieve that, PLL was used to estimate the phase angle $\angle\delta_{gi}$ (where $i \in \{a, b, c\}$) of the grid-side voltage and transform the reference frames of the inputs (i_{gdi_ref} and i_{gqi_ref}) and outputs (i_{gdi} and i_{gqi}) of the current control loop. The inner current control loop is simplified as a low-pass filter with a time constant T_{if} in this study. The inputs to the current control loop were computed from reference active and reactive power (P_{refi} and Q_{refi}) and grid voltage. The Norton current injection was modeled as the interface of GFL inverter to the external grid. The schematic of GFL control for each phase has been presented in Fig. 4.

The responses of the GFM and GFL inverter models have been validated against the detailed EMT models and field test data collected from the Consortium for Electric Reliability Technology Solutions (CERTS)/American Electric Power (AEP) microgrid testbed [1].

C. Grid Support Functions

The inverters were designed to provide autonomous and instant primary control without coordination with others. GFM inverters inherently have droop-based voltage and frequency primary controls to meet certain system operating performances. The primary controls for GFL inverters considered in this study include frequency-watt control and volt-var control, based on droop curves. These functions can be enabled or disabled for GFL inverter as shown in Fig. 4 for GFL inverter. The droop curves for GFM and GFL inverters have been represented in Figs. 5 and 6, respectively. While comparing

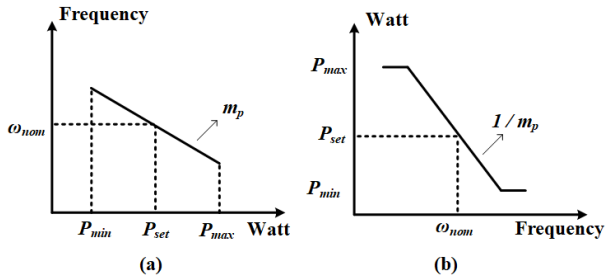

Fig. 5. (a) GFM P–f droop control (b) Freq-Watt for GFL inverter.

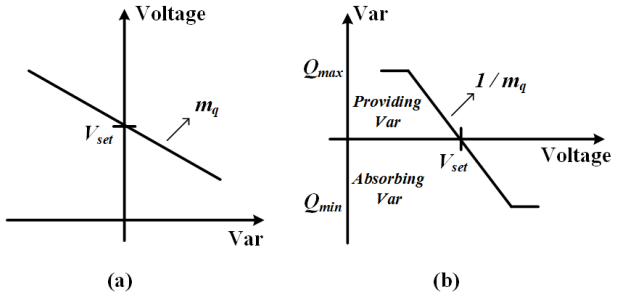

Fig. 6. (a) GFM Q–V droop control (b) Volt-Var for GFL inverter.

Fig. 5 (a) and (b), it is evident that x and y axes have been swapped. Basically, GFM inverter takes active power setpoint P_{set} as input and directly controls grid-side frequency through the P–f droop curve in Fig. 5 (a). In contrast, GFL inverter senses grid-side frequency as input and adjusts its active power reference (P_{ref}) to relieve under- or over- frequency issues. The same explanation applies to the comparison of voltage regulation droop curves of GFM and GFL inverters shown in Fig. 6 (a) and (b), respectively. Fig. 7 shows the control block of the frequency-watt control. It measures the variation of frequency and changes the reference of output power P. The frequency was measured using a PLL. Fig. 8 shows the control block of the volt-var control. It measures the variation of voltage and changes the reference of reactive power Q. In Figs. 7 and 8, time constants T_p and T_q represent the delay of the controllers, while T_f and T_v represent the delay of frequency and voltage measurements.

III. Co-simulation Model Development

This section presents the details of co-simulation model development including theoretical implementation of co-simulation model, co-simulation interface techniques, iterative T&D power flow initialization and dynamic co-simulation, and

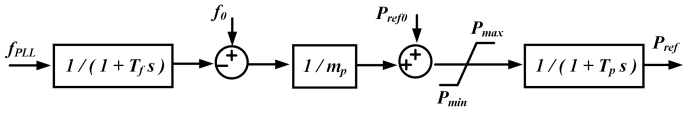

Fig. 7. Grid-following frequency-watt control.

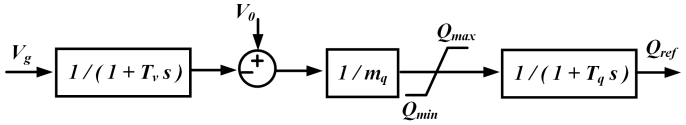

Fig. 8. Grid-following volt-var control.

T&D power grid models. The co-simulation platform consists of three simulation tools. A simple description of each of them is provided below:

- *GridPACK* is a software framework consisting of a set of modules designed to simplify the development of programs that model the transmission power grid and run on parallel HPC platforms. This transmission simulator incorporates several applications including power flow analysis, dynamic simulation, contingency analysis, state estimation, and dynamic state estimation based on Kalman filter [37].
- *GridLAB-D* is a flexible distribution system simulation environment that can be integrated with a variety of third-party data management and analysis tools [28]. GridLAB-D incorporates an extensive suite of tools to build and manage studies including three-phase power flow analysis, QSTS studies, three-phase phasor-domain dynamic simulation running in the timescale of sub-seconds.
- *HELICS* is a flexible and scalable open-source co-simulation framework that integrates simulators designed for separate transmission, distribution and communication domains to simulate regional and interconnection-scale power system behaviors at unprecedented levels of detail and speed. HELICS is designed to run on HPC system and supports a variety of computation platforms and programming languages [38].

A. Implementation of Co-simulation Model

In both transmission and distribution simulators, the phasor-domain dynamic simulation was executed to generate time-domain trajectories. The dynamics for the transmission network can be represented using the following set of differential and algebraic equations.

$$\frac{dx_T(t)}{dt} = f_T(x_T(t), V_T(t)) \tag{9}$$

$$I_T(t) = g_T(x_T(t), I_{D\_bb}(t), V_T(t)) \tag{10}$$

$$V_T(t) = Y_T^{-1} I_T(t) \tag{11}$$

Where $x_T(t)$ represents the dynamic states of the dynamic components in the transmission network, $V_T(t)$ represents the voltages at each bus of the transmission network, $I_T(t)$ indicates the injected currents at each bus, $I_{D\_bb}(t)$ represents the injected currents from distribution network at each boundary bus (noted by bb), and Y_T is the admittance matrix of the transmission network. Eq. (9) represents the differential equations describing the dynamic behaviors of the components in the network. Eqs. (10) and (11) express the network solution of the system. A similar equation set applies to distribution network dynamics as described below.

$$\frac{dx_D(t)}{dt} = f_D(x_D(t), V_D(t), V_{T\_bb}(t)) \tag{12}$$

$$I_D(t) = g_D(x_D(t), V_D(t), V_{T\_bb}(t)) \tag{13}$$

$$V_D(t) = Y_D^{-1} I_D(t) \tag{14}$$

In which, $V_{T\_bb}(t)$ represents substation voltage of each boundary bus received from transmission network. Specific numerical integration methods, such as modified Euler or Trapezoidal integration were applied to discretize the above continuous-time differential equations and turn them into discrete forms suitable for implementation in power system simulators. Usually, in phasor-domain transmission and distribution simulators, a common numerical integration time step at several milli-seconds can be used to guarantee convergence of simulation. In this study, we used regular time step (ΔT) for distribution simulator and relatively smaller time step ($\Delta T/N$) for transmission simulator. In our study, the transmission-side contingency was simulated, and the use of smaller time step in transmission simulator was found to improve the convergence and accuracy of the co-simulation without significantly increasing the computation burden since only one transmission network was present in the co-simulation.

After discretization, the following set of discrete-time equations were derived for transmission network.

$$t_{k+1} = t_k + \frac{\Delta T}{N} \tag{15}$$

$$X_T(t_{k+1}) = F_T(X_T(t_k), V_T(t_k)) \tag{16}$$

$$I_T(t_{k+1}) = G_T(X_T(t_{k+1}), I_{D\_bb}(t_k), V_T(t_k)) \tag{17}$$

$$V_T(t_{k+1}) = Y_T^{-1} I_T(t_{k+1}) \tag{18}$$

In this co-simulation, the transmission simulator was designed to lead the distribution simulator in simulation time. During one regular time step (ΔT), Eqs. (15) - (18) were executed N times before the distribution simulator proceeds by one time step (ΔT). Finally, the boundary bus voltage $V_{T\_bb}(t_{m+1})$ would be sent from GridPACK to GridLAB-D after N time steps. Accordingly, the set of discrete-time equations for distribution system was derived as below.

$$t_m = t_k \tag{19}$$

$$t_{m+1} = t_m + \Delta T \tag{20}$$

$$X_D(t_{m+1}) = F_D(X_D(t_m), V_D(t_m), V_{T\_bb}(t_{m+1})) \tag{21}$$

$$I_D(t_{m+1}) = G_D(X_D(t_{m+1}), V_D(t_m), V_{T\_bb}(t_{m+1})) \tag{22}$$

$$V_D(t_{m+1}) = Y_D^{-1} I_D(t_{m+1}) \tag{23}$$

$$P_{sub}(t_{m+1}) + jQ_{sub}(t_{m+1}) = V_{T\_bb}(t_{m+1}) I^*_{D\_bb}(t_{m+1}) \tag{24}$$

Where $I^*_{D\_bb}(t_{m+1})$ represents the substation current injection at the distribution side of each boundary bus and can be updated using Eq. (22), this current injection finds use at the transmission side to update interface load current injection of each boundary bus by Eq. (17). The substation active and reactive power calculated by Eq. (24) would then be sent from GridLAB-D to GridPACK and converted into current injection internally inside GridPACK. Since the same boundary bus voltage is used on the GridLAB-D and GridPACK sides, this method is equivalent to directly passing the GridLAB-D substation branch current values to the corresponding GridPACK constant current load interface.

The GridPACK and GridLAB-D communicate with each other through HELICS. Fig. 9 presents the interface representation on both sides of the system. On the GridPACK bulk power system side, the interface load is represented by

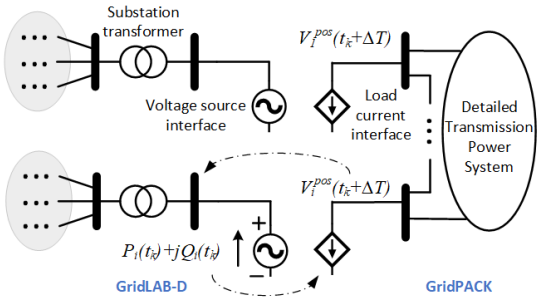

Fig. 9. Interface models on T&D sides.

current injection. On the GridLAB-D distribution systems side, the external grid is modeled as a substation voltage source receiving the positive-sequence voltage magnitude and angle from transmission simulator. At each HELICS communication time step, the GridPACK passes the interface bus complex voltages to each distribution substation and receives the active and reactive power at substation from GridLAB-D. The dynamic simulation of GridPACK transmission system model and many GridLAB-D distribution system models proceeds in a parallel mode in the HPC platform, which enables the high-efficiency integration of a large number of distribution feeders. It is reasonable to assume that no negative- or zero- sequence voltages and currents are transmitted between transmission and distribution systems because of the balanced design of distribution system and *Delta-Y-Gnd* configuration of substation transformer.

B. Initialization and Dynamic Co-simulation

The T&D co-simulation usually requires a satisfactory initialization on both sides of the system to improve the numerical stability and reduce the time for the post-interfacing dynamics to settle down. An iterative T&D power flow initialization approach has been proposed in this study to autonomously adjust and exchange the boundary conditions at the interface buses. Fig. 10 shows the details of the entire T&D co-simulation process, which consists of: (a) iterative power flow initialization and (b) interactive dynamic co-simulation. During the initialization, the transmission network and each distribution feeder solves power flow on the assigned central processing unit (CPU) core in parallel mode. The distribution-side substation P and Q of each feeder was scaled up and compared with the corresponding interface bus load of transmission system. The absolute difference of P and Q was calculated and sent to a comparison block. If the P or Q difference at any feeder substation was found to be greater than a threshold value ϵ, the boundary conditions were exchanged. In this case, the PQ value of each interface bus load in the transmission system was substituted by the corresponding distribution feeder substation scaled PQ, and the positive-sequence voltage magnitude and angle of each interface bus was returned to the corresponding distribution feeder to represent the substation complex voltage. After the exchange of boundary conditions, the power flow on both T and D sides were solved independently and the initialization proceeded to the next iteration. The iterative power flow solution converged when the PQ mismatch at every interface bus was less than the pre-determined threshold ϵ.

After the iterative power flow initialization, the T&D system then started the interactive dynamic co-simulation as depicted in Fig. 10 (b). As previously mentioned, this study used small time step ($\Delta T/N = 1ms$) for the GridPACK transmission system and large time step ($\Delta T = 5ms$) for the GridLAB-D distribution system and HELICS data exchange. The T- and D-side simulation began simultaneously and ran independently on different CPU cores. The co-simulation engine HELICS synchronized the simulation time in GridPACK and GridLAB-D and ensured that all the feeder models strictly followed the transmission model in the time elapse. Fig. 10 (b) shows the detailed co-simulation mechanism of one GridLAB-D time step ΔT. GridPACK and GridLAB-D were synchronized in time at the beginning of current time step ($t_m = t_k$). Each boundary data exchange between the transmission network and distribution feeders was divided into four steps. First, each feeder model sent the substation P_{sub} and Q_{sub} at the beginning of the current time step to the corresponding interface load bus in the transmission system. Thereafter, the transmission simulation moved forward for $N = 5$ small time steps and updated the bus voltage magnitude and angle. This was followed by the transmission simulator sending out the updated complex voltage V_{T_bb} of each interface boundary bus to the corresponding feeder substation at the end of the current time step. Lastly, after receiving the updated substation voltages, all the feeder models moved ahead by one time step ΔT. In this study, the loosely-coupled T&D dynamic co-simulation was utilized to guarantee simulation speed while maintaining accuracy. Using this data exchange sequence, the distribution-side GridLAB-D simulation lagged the transmission-side GridPACK simulation by one GridLAB-D time step (ΔT).

C. Power Grid Models

The mini-WECC system [34] was used as the base-case transmission system for all the multiple scenarios with different IBR penetration level and different GFL/GFM percentage. Generation for many areas of the WECC system was equivalenced into multiple generators in the mini-WECC system and key generators in the original WECC system were maintained in the model. System loads were lumped into major metropolitan areas. The mini-WECC system model was simulated with the dynamic simulation engine of GridPACK. All the loads in the mini-WECC system were replaced with the 8500-node detailed feeder models developed in GridLAB-D in the T&D co-simulation. The IEEE 8500-node test feeder represents a large radial distribution feeder which provides a challenging circuit for distribution studies. The 8500-node test feeder includes many elements that may be found on a North American medium voltage (MV) distribution feeder, such as multiple feeder regulators, per-phase capacitor control, feeder secondaries, and service transformers [39]. Fig. 11 gives the single line diagram of the mini-WECC system and IEEE 8500 node test feeder. A scaling factor is applied to scale up the total power at feeder substation to match the

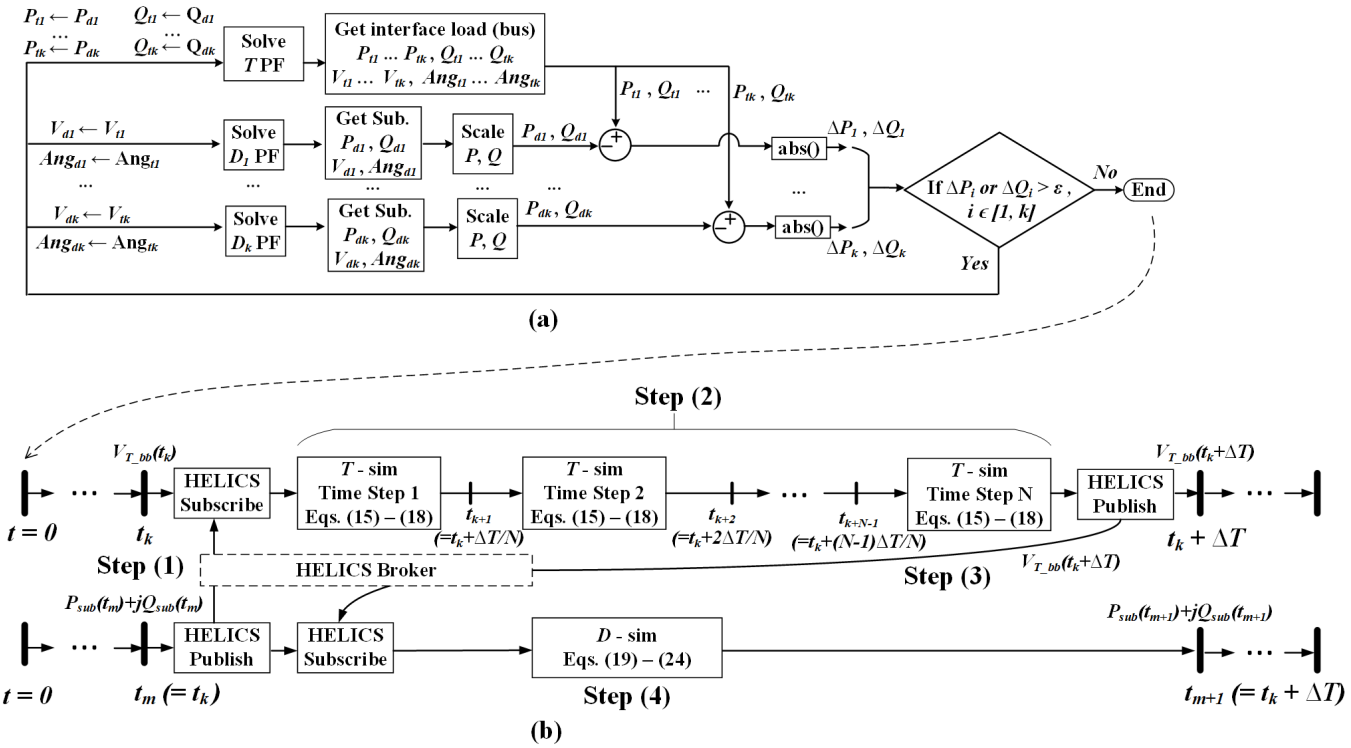

Fig. 10. Initialization and co-simulation - (a) iterative T&D power flow initialization, (b) interactive dynamic co-simulation (Note: sub. → substation).

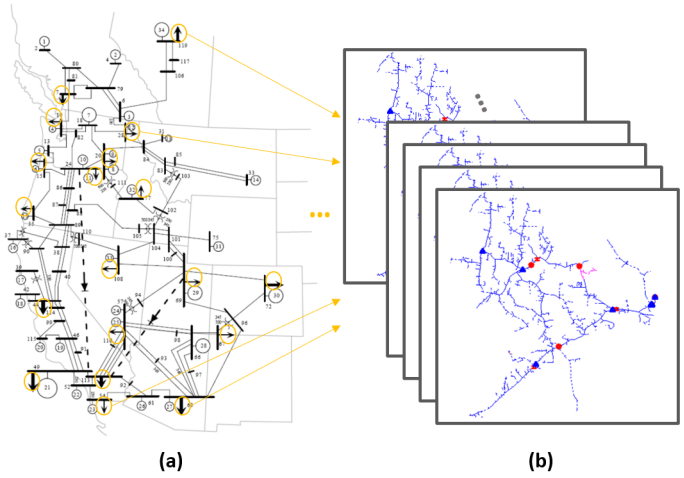

Fig. 11. Power grid models. (a) mini-WECC, (b) 19 modified IEEE 8500 node feeders.

transmission load level in the mini-WECC system, virtually representing many identical 8500-node feeders connected to the same transmission load bus.

IV. Simulation and Results

In this section, the simulation cases were set up and the results have been discussed. The co-simulation platform reported in this study was built and installed on a Linux Ubuntu machine linked to PNNL's HPC resources. All the 19 loads in the mini-WECC system were interfaced with IEEE 8500-node feeder models. The substation P of each distribution feeder model was scaled up by a multiplier to match the corresponding interface load P in the transmission

TABLE II
Iterative T&D power flow solution at Bus 8

itr.	Pload (MW)	Qload (MVAr)	Vmag (pu)	Vang (deg)
1	1090.584	268.008	1.017137	-6.52382
2	1090.584	40.86753	1.034768	-6.44766
3	1090.584	42.52485	1.034644	-6.44811
4	1090.584	42.51928	1.034645	-6.44811
5	1090.584	42.5193	1.034645	-6.44811
6	1090.584	42.5193	1.034645	-6.44811

system. The Q of the feeder model was multiplied by the same scaling factor to represent interface load Q. In each feeder model, 550 IBRs were distributed randomly and operated at several kilo-watts for each unit. Therefore, the developed T&D co-simulation platform reported in this study had the capacity to simulate up to 10,450 detailed inverter models, which described the highest scalable model reported compared to other similar studies and has the capabilities for further expansion using additional CPU cores and larger-scale grid models.

A. Voltage and Frequency Responses without Transmission-Side IBR Penetration

In the first simulation scenario, the transmission-side IBRs were not modeled. The 275 grid-forming inverters shown in Fig. 3 and 275 grid-following inverters shown in Fig. 4 were modeled in each IEEE 8500-node feeder. The mini-WECC system had 34 synchronous generators with exciter and governor models. The largest generator at Bus 48 was tripped. The iterative T&D power flow initialization was performed, followed by the T&D dynamic co-simulation.

This article has been accepted for publication in IEEE Transactions on Power Delivery. This is the author's version which has not been fully edited and content may change prior to final publication. Citation information: DOI 10.1109/TPWRD.2023.3302303

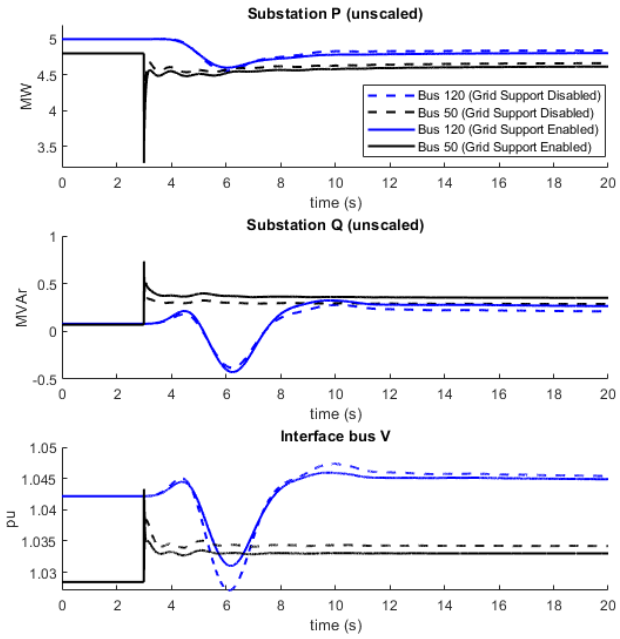

Fig. 12. Unscaled active and reactive power and voltage magnitude at the substations of selected interface buses (positive PQ indicates net power consumed by feeder).

TABLE II demonstrates the convergence of the iterative power flow initialization at Bus 8. The load bus P was always matched by multiplying the feeder substation P with a dynamic scaling factor. Therefore, the P was almost unchanged. The iterative T&D power flow takes 6 iterations to converge. The final scaling factor at the last iteration will be used in the dynamic co-simulation to scale up substation P and Q, and the transmission-side interface load PQ at the last iteration will be used as the initial load condition in the dynamic co-simulation.

Fig. 12 presents the unscaled active and reactive power and voltage magnitude at the substations of the selected 2 interface buses, including a bus (Bus 50) adjacent to the location of tripped generator and a bus (Bus 120 in Northeast Alberta area) with weak interconnection with the rest of WECC system. In Fig. 12, if the grid support functions are enabled, in response to the generator tripping, GFL inverters would slightly increase P output (reflected by lower substation P consumption) to boost the depressed frequency and decrease Q output (reflected by higher substation Q consumption) to lower the raised voltage magnitude in response to the generator tripping.

In addition to the above scenario with 10,450 inverters (5,225 GFM + 5,225 GFL), the study also covers the scenarios with only 5,225 GFM inverters, only 5,225 GFL inverters, and the scenario with no inverters. For the scenarios involving GFL inverters, the performances of enabling and disabling grid support functions were compared. The frequency at Bus 59 was plotted under these scenarios, as shown in Fig. 13. It can be seen that the scenarios with 5,225 GFL inverters (grid support disabled) and with no inverters exhibit the worst frequency responses because the GFL inverters use constant current control, so they don't respond to frequency changes. The scenario with 5,225 GFL inverters (grid support enabled)

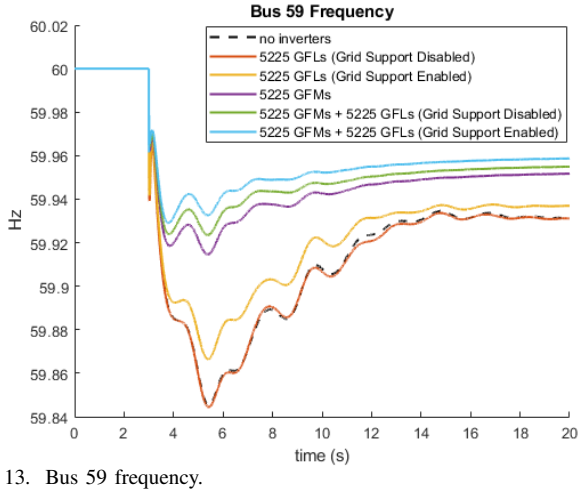

Fig. 13. Bus 59 frequency.

has better frequency response. The frequency responses in the scenarios with GFM inverters are much better than those without GFM inverters. The scenario with 10,450 inverters (GFL grid support enabled) has the lightest net load at each interface bus, therefore the frequency response is the best. The observations corroborate the conclusion that the GFM inverters can provide much better primary frequency regulation during an under-frequency event compared to GFL inverters with grid support functions enabled.

B. GFM Penetration Study

This subsection describes the results of the investigation to estimate the minimum required penetration of GFM inverters to maintain dynamic stability under different IBR penetration levels. The grid support functions of distribution-side GFL inverters were disabled in this part of study. TABLE III gives the different penetration level of IBRs for the multiple scenarios created for this co-simulation system. As shown in TABLE III, the total IBR penetration level in the T&D co-simulation system increased gradually from 0% (all synchronous machines as the energy resources) to 100% (all IBRs as the energy resources) with a total of nine different scenarios. And for each scenario, the IBR resources were evenly split on the transmission and distribution sides. The bulleted points below explain the changes made on the base case to formulate the cases of different IBR penetration.

- For all the designed scenarios in TABLE III, the total amount of consumer loads in the T&D co-simulation system remained the same.
- The distribution system IBR penetration level increased with the increase in power rating of 550 IBRs in each distribution feeder, and the percentage of the distribution system IBR penetration level corresponds to the total consumer loads in scenario 1 (base case).
- The transmission system IBR penetration level increased when the synchronous machines are replaced with IBRs. For a specific IBR penetration level, in addition to the replacement of synchronous machines with IBRs at the transmission system, a certain percentage of additional synchronous machines must be shut down to balance the net load reduction with certain penetration of IBRs in the

TABLE III
IBR PENETRATION LEVELS FOR DIFFERENT T&D CO-SIMULATION SCENARIOS

Scenario No.	Total IBR penetration level	Transmission system IBR penetration level	Distribution system IBR penetration level
1	0% (base case)	0% (base case)	0% (base case)
2	20%	10%	10%
3	40%	20%	20%
4	50%	25%	25%
5	60%	30%	30%
6	70%	35%	35%
7	80%	40%	40%
8	90%	45%	45%
9	100%	50%	50%

TABLE IV
MINIMUM PERCENTAGE OF GFM NEEDED FOR STABLE SYSTEM OPERATION FOR DIFFERENT PENETRATION OF IBRS

Total system IBR penetration	Share of GFL inverters in IBRs			
	Around 85%	Around 90%	Around 95%	Around 100%
20%				100% GFL
40%				100% GFL
50%				100% GFL
60%				100% GFL
70%				100% GFL
80%			95.3% GFL 4.7% GFM	100% GFL
90%		91.3% GFL 8.7% GFM	95.3% GFL 4.7% GFM	
100%	87.9% GFL 12.1%	89.8% GFL 10.2%		

distribution system, as IBRs in the distribution system tend to reduce the net-load "seen" from the transmission side for the distribution feeders. For example, for the scenario No. 6, which has a total of 70% IBR penetration level, a total of 35% of synchronous machines in the transmission system were replaced by the IBRs, as well as another 35% of synchronous machines in the transmission system were shut down to balance the 35% net load reduction caused by the 35% IBR penetration at the distribution systems. Simply speaking, 35% generation (measured by total MW capacity in the base case) was shifted from transmission system to distribution system and was contributed to by the 10,000+ distributed inverters.

For each scenario shown in TABLE III, the minimum required percentage of GFM inverters was investigated for the certain IBR penetration level that can sustain the stable frequency response of the system. For the IBRs in the distribution feeders, it was assumed that the IBRs were customer-owned and had small power rating (around 10kW for each IBR) and had simple GFL controls described in Fig. 4. For the IBRs in the transmission system, we assume these IBRs are utility-scale IBRs and thus can either be GFL or GFM inverters as described in Section II-A.

For each scenario, a T&D co-simulation was run with a total simulation time of 20.0 seconds, with a disturbance of the largest generator (at Bus 48) tripped at 5.0 second of the co-simulation. For a certain scenario shown in TABLE III, we first examined the case wherein all the IBRs in the transmission system were modeled as GFL inverters and the co-simulation was run to check whether the system could experience a stable frequency response after the disturbance. If the system suffered stability issues with 100% GFL inverters for a certain IBR penetration level scenario, we gradually increased the percentage of the GFM models in the scenario and re-ran the T&D co-simulation to check whether the system response becomes stable. With this trial-and-error method, we found the minimum required percentage of GFM inverters to sustain the stable frequency response of the system for each scenario with different IBR penetration level, as shown in TABLE IV, where a "green" block in the table means that the certain percentage of GFL inverters for the certain IBR penetration scenario had been tested with co-simulation and the system frequency response was stable, while a "red" block in the table meant the system frequency response was not stable after testing the specific combination of IBR and GFL percentage.

Fig. 14 shows the frequency response of the T&D co-simulation for the IBR penetration scenarios from 0% to 80% in TABLE III with 100% of GFL inverters under the disturbance of Bus 48 generator tripping. Fig. 15 shows the frequency response of the T&D co-simulation for the IBR penetration scenarios from 80% to 100% in TABLE III, with the minimum required share percentage of GFM inverters to sustain a stable frequency response for that scenario.

The following observations are highlighted from the above results:

1) As shown in TABLE IV, the T&D system can maintain a stable response with 100% share of GFL inverters for the total IBR penetration level up to 70%. GFM inverters are needed to sustain system's stable frequency response when the total IBR penetration level is higher than 70%. Higher percentage of GFM inverters are needed to sustain the system's stable frequency response when the total IBR penetration level increases from 80% to 100%.
2) As shown in Fig. 14, the frequency nadir decreases when the total IBR penetration level of the T&D system increases from 0% to 70% with 100% share of GFL inverters. This is expected since the primary frequency response support of system is reduced with the percentage of the synchronous machine decreasing in the system while the GFL inverters can only provide very limited primary frequency response in its control logic.
3) As shown in Fig. 15, the system frequency nadir increases when the total IBR penetration level of the T&D system increases from 80% to 100% with GFM inverters added in the system. This is expected since the GFM inverters provide fast primary frequency response support for the system.
4) As shown in Fig. 14 and Fig. 15, compared with synchronous machines, the GFM inverters provide much faster and better primary frequency response support for the system, due to its very fast control with power electronics devices. Fig. 15 shows that, for the 100% IBR penetration scenario without any synchronous machine,

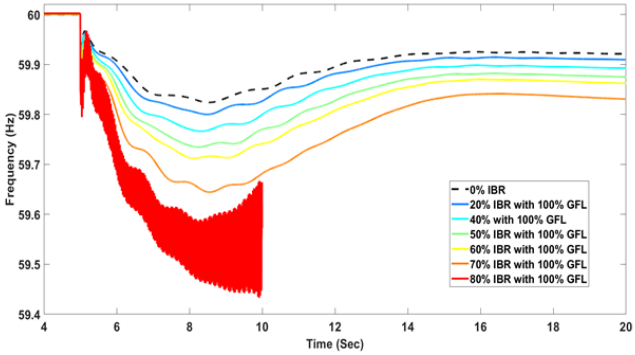

Fig. 14. Frequency response of the T&D co-simulation for each different IBR penetration scenario (0% to 80%) with 100% share of GFL inverters.

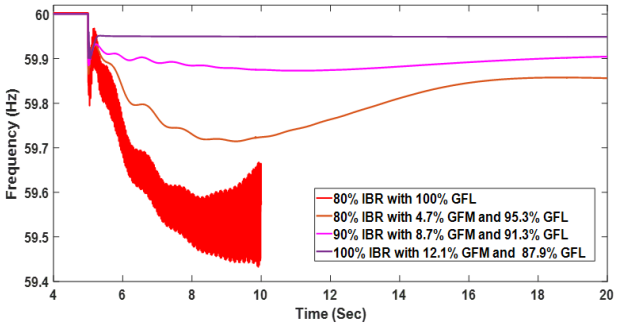

Fig. 15. Frequency response of the T&D co-simulation for each different IBR penetration scenario (80% to 100%) with minimum required share of GFM inverters to sustain a stable response.

only 12% of GFM inverters are needed to guarantee a stable frequency response, and the frequency nadir of the 12% GFM for 100% IBR penetration scenario is much higher than the base-case with 100% synchronous machines (0% IBR) as shown in Fig. 14.

5) For 100% IBR scenario in Fig. 15, the frequency response appears to effectively "snap" to a new value. This scenario has the highest percentages of GFM inverters, and no synchronous machines exist in the system. This clean step change in frequency is observed in the hardware testing results done by grid-forming inverter manufacturers on a small system [40].

V. Conclusions

This study presents a large-scale T&D dynamic co-simulation platform connecting the mini-WECC system with 19 IEEE 8500-node distribution feeders, integrating more than 10,000 real-size GFM and GFL inverters. The platform was developed based on open-source T&D simulators (GridPACK & GridLAB-D) and a highly-scalable co-simulation engine HELICS, and was linked to PNNL's HPC resources to facilitate parallel simulation. An iterative T&D power flow initialization approach was proposed in this study to guarantee smooth transition from power flow mode to dynamic co-simulation mode. The simulation results verify that though the GFL inverters with grid support functions can provide limited frequency support, the aggregate effect of small-scale GFM inverters can result in noticeable amount of primary frequency response to the bulk power grid. If 100% inverters are GFL-controlled, the IBR penetration will be capped by a specific percentage to maintain system stability. However, if a small portion (around 12% in this study) of GFL inverters are replaced with GFM inverters, the IBR penetration can reach 100%.

The developed platform can also be used to study complex phenomena which cannot be simulated using aggregate inverter models, wherein the impacts of inverters with mixed control strategies, the effects of inverter location on distribution systems, and the impact of wide-spread momentary cessation or tripping of inverters can be better understood.

References

[1] W. Du, F. K. Tuffner, K. P. Schneider, R. H. Lasseter, J. Xie, Z. Chen, and B. Bhattarai, "Modeling of grid-forming and grid-following inverters for dynamic simulation of large-scale distribution systems," *IEEE Trans. Power Del.*, vol. 36, no. 4, pp. 2035–2045, 2021.

[2] Y. Li, S. Hu, X. Zhang, and P. Tian, "Dynamic equivalent of inverter-based distributed generations for large voltage disturbances," *Energy Reports*, vol. 8, pp. 14 488–14 497, 2022.

[3] P. Sowa and D. Zychma, "Dynamic equivalents in power system studies: A review," *Energies*, vol. 15, 2022.

[4] T. Rabuzin, R. Eriksson, and L. Nordström, "Model structure selection and validation for dynamic equivalencing of distribution networks," *IEEE Trans. Smart Grid*, vol. 13, no. 2, pp. 1347–1356, 2022.

[5] E. O. Kontis, T. A. Papadopoulos, M. H. Syed, E. Guillo-Sansano, G. M. Burt, and G. K. Papagiannis, "Artificial-intelligence method for the derivation of generic aggregated dynamic equivalent models," *IEEE Trans. Power Syst.*, vol. 34, no. 4, pp. 2947–2956, 2019.

[6] F. Conte, F. D'Agostino, S. Massucco, G. Palombo, F. Silvestro, C. Bossi, and M. Cabiati, "Dynamic equivalent modelling of active distribution networks for tso-dso interactions," in *2017 IEEE PES Innovative Smart Grid Technologies Conference Europe (ISGT-Europe)*, 2017, pp. 1–6.

[7] B. Badrzadeh. Is electromagnetic transient modelling and simulation of large power systems necessary and practical? [Online]. Available: https://www.esig.energy/is-electromagnetic-transient-modelling-and-simulation-of-large-power-systems-necessary-and-practical/

[8] S. Ciraci, J. A. Daily, J. C. Fuller, A. R. Fisher, L. D. Marinovici, and K. Agarwal, "FNCS: A framework for power system and communication networks co-simulation," 4 2014. [Online]. Available: https://www.osti.gov/biblio/1156991

[9] "Hierarchical engine for large-scale infrastructure co-simulation, version 00," 4 2017. [Online]. Available: https://www.osti.gov/biblio/1352903

[10] S. M. Mohseni-Bonab, A. Hajebrahimi, I. Kamwa, and A. Moeini, "Transmission and distribution co-simulation: A review and propositions," *IET Gener. Transm. Distrib.*, vol. 14, no. 21, pp. 4631–4642, 2020.

[11] Q. Huang, R. Huang, R. Fan, J. Fuller, T. Hardy, Z. Huang, and V. Vittal, "A comparative study of interface techniques for transmission and distribution dynamic co-simulation," in *2018 IEEE PES General Meeting (PESGM)*, 2018, pp. 1–5.

[12] K. Balasubramaniam and S. Abhyankar, "A combined transmission and distribution system co-simulation framework for assessing the impact of volt/var control on transmission system," in *2017 IEEE PES General Meeting*, 2017, pp. 1–5.

[13] J. Yip, Q. Nguyen, and S. Santoso, "Analysis of effects of distribution system resources on transmission system voltages using joint transmission and distribution power flow," in *2020 IEEE PES General Meeting*, 2020, pp. 1–5.

[14] A. K. Bharati and V. Ajjarapu, "Investigation of relevant distribution system representation with DG for voltage stability margin assessment," *IEEE Trans. Power Syst.*, vol. 35, no. 3, pp. 2072–2081, 2020.

[15] H. Jain, B. Palmintier, I. Krad, and D. Krishnamurthy, "Studying the impact of distributed solar PV on power systems using integrated transmission and distribution models," in *2018 IEEE/PES Transm. and Distr. Conf. and Expo. (T&D)*, 2018, pp. 1–5.

[16] B. Palmintier, E. Hale, T. M. Hansen, W. Jones, D. Biagioni, H. Sorensen, H. Wu, and B.-M. Hodge, "IGMS: An integrated iso-to-appliance scale grid modeling system," *IEEE Trans. Smart Grid*, vol. 8, no. 3, pp. 1525–1534, 2017.

[17] N. Panossian, T. Elgindy, B. Palmintier, and D. Wallison, "Synthetic, realistic transmission and distribution co-simulation for voltage control benchmarking," in *2021 IEEE Texas Power and Energy Conference (TPEC)*, 2021, pp. 1–5.

[18] R. Sadnan, G. Krishnamoorthy, and A. Dubey, "Transmission and distribution (T&D) quasi-static co-simulation: Analysis and comparison of t&d coupling strength," *IEEE Access*, vol. 8, pp. 124 007–124 019, 2020.

[19] G. Krishnamoorthy and A. Dubey, "Transmission–distribution cosimulation: Analytical methods for iterative coupling," *IEEE Syst. J.*, vol. 14, no. 2, pp. 2633–2642, 2020.

[20] R. Venkatraman, S. K. Khaitan, and V. Ajjarapu, "Application of combined transmission-distribution system modeling to WECC composite load model," in *2018 IEEE PES General Meeting*, 2018, pp. 1–5.

[21] ——, "Dynamic co-simulation methods for combined transmission-distribution system with integration time step impact on convergence," *IEEE Trans. Power Syst.*, vol. 34, no. 2, pp. 1171–1181, 2019.

[22] R. W. Kenyon, B. Mather, and B.-M. Hodge, "Coupled transmission and distribution simulations to assess distributed generation response to power system faults," *Elect. Power Syst. Res.*, vol. 189, 2020.

[23] M. M. Rezvani, S. Mehraeen, J. R. Ramamurthy, and T. Field, "Dynamic interaction of distribution-connected DER_A with transmission system via co-simulation analysis," *IEEE Trans. Ind. Appl.*, vol. 58, no. 2, pp. 1502–1511, 2022.

[24] A. K. Bharati and V. Ajjarapu, "SMTD co-simulation framework with HELICS for future-grid analysis and synthetic measurement-data generation," *IEEE Trans. Ind. Appl.*, vol. 58, no. 1, pp. 131–141, 2022.

[25] W. Wang, X. Fang, H. Cui, F. Li, Y. Liu, and T. J. Overbye, "Transmission-and-distribution dynamic co-simulation framework for distributed energy resource frequency response," *IEEE Trans. Smart Grid*, 2021.

[26] R. Huang, R. Fan, J. Daily, A. Fisher, and J. Fuller, "An open-source framework for power system transmission and distribution dynamics co-simulation," *IET Gener. Transm. Distrib.*, vol. 11, no. 12, pp. 3152–3162, 2017.

[27] GridPACK^{TM}: An open source toolkit for developing power grid simulation applications for high performance computing architectures. [Online]. Available: https://www.gridpack.org/wiki/index.php/Main_Page

[28] GridLAB-D^{TM}: A unique tool to design the smart grid. [Online]. Available: https://www.gridlabd.org/

[29] D. Shu, X. Xie, Q. Jiang, Q. Huang, and C. Zhang, "A novel interfacing technique for distributed hybrid simulations combining emt and transient stability models," *IEEE Trans. Power Del.*, vol. 33, no. 1, pp. 130–140, 2018.

[30] Q. Huang and V. Vittal, "Application of electromagnetic transient-transient stability hybrid simulation to FIDVR study," *IEEE Trans. Power Syst.*, vol. 31, no. 4, pp. 2634–2646, 2016.

[31] ——, "Integrated transmission and distribution system power flow and dynamic simulation using mixed three-sequence/three-phase modeling," *IEEE Trans. Power Syst.*, vol. 32, no. 5, pp. 3704–3714, 2017.

[32] H. Wang, Y. Song, S. Huang, Y. Chen, D. Jiao, and Y. Qian, "Hybrid transient simulation platform for interconnected transmission and distribution system based on powerfactory and PSASP," *J. Eng.*, vol. 2017, no. 13, pp. 2053–2056, 2017.

[33] Q. Huang and V. Vittal, "Advanced emt and phasor-domain hybrid simulation with simulation mode switching capability for transmission and distribution systems," *IEEE Trans. Power Syst.*, vol. 33, no. 6, pp. 6298–6308, 2018.

[34] D. Trudnowski and J. Undrill, "Appendix 2: The MinniWECC System Model of Oscillation Damping Controls," Year 1 report of BPA contract 37508, Tech. Rep., 2008.

[35] "Brief summary of all 2nd generation generic renewable energy system dynamic models," 2 2021. [Online]. Available: https://www.wecc.org/Reliability/WECC_RES_Models_Rev5_042321.pdf

[36] W. Du, Y. Liu, F. K. Tuffner, R. Huang, and Z. Huang, "Model specification of droop-controlled, grid-forming inverters (GFMDRP_A)," 12 2021.

[37] GridPACK^{TM}: An open source framework for developing high performance computing simulations of the power grid. [Online]. Available: https://www.pnnl.gov/gridpack/technical-approach

[38] HELICS documentation. [Online]. Available: https://docs.helics.org/en/latest/index.html#

[39] R. F. Arritt and R. C. Dugan, "The IEEE 8500-node test feeder," in *IEEE PES T&D 2010*. IEEE, 2010, pp. 1–6.

[40] A. Knobloch, C. Hardt, A. Falk, T. Bülo, S. Scheurich, C. Khalfet, R. Hesse, T. Becker, and R. Bhattia, "Synchronous energy storage system with inertia capabilities for angle, voltage and frequency stabilization in power grids," in *11th Solar & Storage Power System Integration Workshop (SIW 2021)*, vol. 2021, 2021, pp. 71–78.

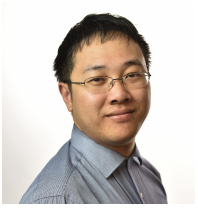

Yuan Liu (Member, IEEE) received a MS and PhD in electrical engineering from Arizona State University in 2012 and 2016. He is a senior research engineer at Pacific Northwest National Laboratory since 2016. His research interests include renewable energy integration, load modeling, and power system simulation and control.

Renke Huang (Senior Member, IEEE) received a PhD in electrical and computer engineering from the Georgia Institute of Technology in 2015. He was a staff research engineer at Pacific Northwest National Laboratory from 2015 to 2022. He is an associate professor at Shanghai Jiao Tong University since 2022. His research interests include power systems modeling, simulation, and control.

Wei Du (Senior Member, IEEE) received a PhD in electrical engineering from Tsinghua University in 2014. He was a visiting student with the University of Wisconsin-Madison from 2012 to 2013. He is currently a staff research engineer at Pacific Northwest National Laboratory. He worked as a research engineer in the key Real Time Digital Simulation Laboratory on power systems at the China Southern Power Grid Company from 2014 to 2016. He worked as a research associate at the University of Wisconsin-Madison from 2016 to 2018. His research interests include microgrids, distribution systems, control of inverter-based resources, hardware-in-the-loop simulation, power system dynamic modeling and analysis, and control of HVDC and FACTS.

Ankit Singhal (Member, IEEE) received a BTech in electrical engineering from the Indian Institute of Technology (IIT) in 2013 and a PhD degree in electrical engineering from Iowa State University in 2019. He worked as a senior power system research engineer at Pacific Northwest National Laboratory from 2019 to 2022. Currently, he is working as an assistant professor in the Department of Electrical Engineering at IIT Delhi. His research interests include modeling, simulation, and control of power distribution systems with distributed energy resources integration. He works on developing models and controls for grid-forming and grid-following inverters, solar PV, electric vehicle, and storage devices to analyze their impact on the power system.

Zhenyu (Henry) Huang (Fellow, IEEE) received his BEng from Huazhong University of Science and Technology in 1994 and a PhD from Tsinghua University in 1999, both in electrical engineering. He is Laboratory Fellow at Pacific Northwest National Laboratory and holds a joint appointment of research professor at Washington State University. He is also a policy advisor on grid modernization for the Department of Energy's Undersecretary for Science and Innovation. He was a technical advisor at the DOE Office of Energy Efficiency and Renewable Energy's Solar Energy Technologies Office in 2019 - 2020. At PNNL, Huang is leading the power electronics and renewable integration portfolios. His research interests include high-performance computing, data analytics, and optimization and control for inverter- and renewable-dominant power and energy systems. Huang has over 200 peer-reviewed publications. Prior to joining PNNL in 2003, Huang conducted extensive research on power system stability and harmonics at the University of Alberta, McGill University, and the University of Hong Kong.